Thermally induced spin torque and domain-wall motion in superconductor/antiferromagnetic-insulator bilayers

G. A. Bobkov,[1] I. V. Bobkova,[2,1,3] A. M. Bobkov,[2] and Akashdeep Kamra[4]
[1]*Moscow Institute of Physics and Technology, Dolgoprudny, 141700 Russia*
[2]*Institute of Solid State Physics, Chernogolovka, Moscow reg., 142432 Russia*
[3]*Dubna State University, Dubna, 141980, Russia*
[4]*Center for Quantum Spintronics, Department of Physics, Norwegian University of Science and Technology, NO-7491 Trondheim, Norway*

(Received 14 December 2020; revised 2 February 2021; accepted 1 March 2021; published 11 March 2021)

We theoretically investigate domain-wall motion in an antiferromagnetic-insulator layer caused by thermally generated spin currents in an adjacent spin-split superconductor layer. An uncompensated antiferromagnet interface enables the two crucial ingredients underlying the mechanism—spin splitting in the superconductor and absorption of spin currents by the antiferromagnet. Treating the superconductor using the quasiclassical theory and the antiferromagnet via Landau-Lifshitz-Gilbert description, we find domain-wall propagation along the thermal gradient with relatively large velocities $\sim$100 m/s. Our proposal exploits the giant thermal response of spin-split superconductors in achieving large spin torques towards driving domain wall and other spin textures in antiferromagnets.

DOI: 10.1103/PhysRevB.103.094506

I. INTRODUCTION

Recent advancements in stabilizing and manipulating textured magnetic states has led to a paradigmatic transition in the role of magnets in futuristic solid state devices [1,2]. In addition to being passive memory storage elements, spin textures may allow for an active participation of magnets in data processing [3]. These continued advancements, however, rely on realizing effective methods to manipulate these spin textures, such as a domain wall (DW). A wide range of methods, from external magnetic field [4] to thermal spin transfer torque [5–11], have been considered as candidates controlling DW motion in ferromagnets. The finite net magnetization in a ferromagnet turns out crucial in nearly all of these mechanisms. On the other hand, antiferromagnet (AFs) offer various advantages due to their fundamentally different and faster dynamics [12–16], but lack net magnetization and the associated easy control. In the context of DW motion, AFs support significantly larger DW velocities thereby offering a faster operation of devices [2,17–19].

Temperature gradient as a drive for DW motion has gained fresh impetus on account of several novel spin-thermal effects discovered in recent years [8,9,20–22]. Thermal gradient encompasses a broad range of mechanisms that could induce DW motion such as electronic spin current generation [9], magnonic spin currents [10,11,23], entropic spin torques [24–27], and so on. Furthermore, there are competing processes at play within these mechanisms resulting in a complex interplay. For example, magnons in a ferromagnet may push a DW away on reflection via linear momentum delivery [28]. Alternately, they may pull the DW in the direction of their origin on transmission and angular momentum delivery [23]. This competition between pull and push forces is still more complex for AFs due to a varying spin of the magnons [29,30]. On the other hand, entropic torques tend to drive DWs towards the hotter end in both ferro- and antiferromagnets [25–27]. Hence, thermally induced spin torques and DW motion in (antiferro)magnets constitutes a subject with intriguing physics [22,31], in addition to a high technological relevance.

Various thermoelectric (spin) effects in normal or magnetic metals are small because they scale as temperature divided by the Fermi energy, with the latter being a large quantity [8,32,33]. This smallness of thermoelectric effects can be overcome in superconductors where the superconducting gap, or equivalently the critical temperature, replaces the Fermi energy as the relevant parameter [32,33]. Thus, giant thermoelectric effects and thermal spin currents can be achieved in hybrids comprising superconductor (S) and ferromagnet (F) layers [32–37]. The two key ingredients in achieving such giant effects are spin splitting of quasiparticle density of states in the superconductor [38,39] and spin-resolved transport. Both of these are accomplished in S/F hybrids [40,41]. As a result, a giant thermally induced quasiparticle spin current and DW velocities in the latter are possible and have recently been predicted [42]. The recent prediction of spin splitting induced in S by an adjacent AF insulator bearing an uncompensated interface [43] raises the question if a similar thermal spin current and DW motion can be realized in S/AF hybrids, which constitutes the subject of this paper. Such uncompensated moments at AF surfaces have been observed in numerous experiments [44–52]. Furthermore, a variety of effects that are highly sensitive to the nature of the interface with an AF have been predicted recently [53–57].

We theoretically investigate an S/AF bilayer in which the AF hosts a DW and bears an uncompensated interface with S such that only one of the two sublattices in AF is exposed

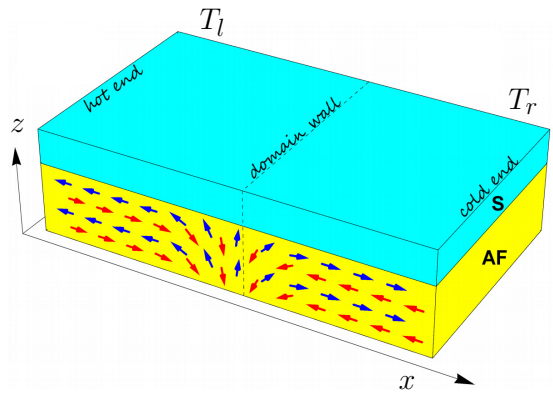

FIG. 1. System under consideration: superconductor/antiferromagnet (S/AF) bilayer with uncompensated magnetic moment at the S/AF interface. Blue arrows depict spin of the A sublattice atoms, while red arrows correspond to the B sublattice. The temperature difference $T_l - T_r$ is applied along the x direction.

to S [43,58]. This results in a finite and spatially varying exchange field in S. We find that subjecting the hybrid to a thermal gradient primarily results in a large quasiparticle spin current in S. The latter exerts spin torque on the AF DW and moves it along the direction of the thermal gradient with velocities ∼100 m/s. We evaluate the thermally generated spin currents in S microscopically using quasiclassical theory and treat the dynamics in AF using the two-sublattice Landau-Lifshitz-Gilbert description. Besides numerically analyzing the ensuing response and DW velocities in a broad parameter space, we also derive analytic expressions in the limit of small DW width. Our analysis further provides guidance to experiments in optimizing the spin splitting and thermal gradients that realize the highest DW velocities.

II. MODEL AND OVERVIEW

The model system that we consider is shown in Fig. 1. It is a thin film bilayer consisting of an antiferromagnetic-insulator AF hosting a domain wall interfaced to a conventional spin-singlet superconductor S. We assume uncompensated magnetic moments at the S/AF interface, that is the interface possesses finite magnetization. The hybrid is subjected to a thermal gradient by connecting it to two thermal reservoirs maintained at different temperatures.

Under these conditions we expect the uncompensated AF to induce a spin splitting in the superconductor [43] via an interfacial exchange interaction. The thermal gradient in such a spin-split superconductor gives rise to a giant spin-dependent Seebeck effect [32–34]. The ensuing spin current, constituted largely by the quasiparticles, exerts a spin torque on the AF via the interfacial exchange interaction resulting in domain-wall motion.

We treat S within the quasiclassical framework and solve the Eilenberger equation to obtain physical quantities. The AF insulator is treated via the two-sublattice Landau-Lifshitz-Gilbert (LLG) description. The two subsystems are coupled due to the interfacial exchange, assumed between S and the sublattice A. This leads to a spin-splitting term in the Eilenberger equation describing S and a spin torque term describing the magnetization dynamics for the AF sublattice A. The overall system dynamics is determined by solving the coupled equations self-consistently.

In the first part we determine the physical observables, such as spin current in the superconductor, via a numerical solution of the Eilenberger and LLG equations. This analysis follows a methodology similar to the recent study of superconductor/ferromagnet bilayers [42]. In the second part we solve Eilenberger equation analytically obtaining expression for spin torque. Following collective coordinates approach for describing the domain wall [17], this allows us to obtain analytic expression for the velocity. The latter result allows a systematic analysis of physical conditions that would optimize the domain-wall velocities.

A. Magnetization dynamics in the antiferromagnet

The Landau-Lifshitz-Gilbert (LLG) equation can be written for each sublattice separately [59]:

$$\frac{\partial \boldsymbol{m}_i}{\partial t} = -\gamma \boldsymbol{m}_i \times \boldsymbol{H}^i_{\rm eff} + \sum_j \alpha_{ij} \boldsymbol{m}_i \times \frac{\partial \boldsymbol{m}_j}{\partial t} + \boldsymbol{N}_i, \tag{1}$$

where $\boldsymbol{m}_i = \boldsymbol{M}_i/M$ is the unit vector aligned with the sublattice magnetization $\boldsymbol{M}_i$, M is the sublattice saturation magnetization, $i = A, B$ is the sublattice index, and γ is the gyromagnetic ratio magnitude. α_{ij} is the 2×2 Gilbert dissipation matrix [59,60], which can be characterized by two real positive numbers α and α_c as follows: $\alpha_{AA} = \alpha_{BB} = \alpha$ and $\alpha_{AB} = \alpha_{BA} = \alpha_c$. The last term in Eq. (1) represents the torque experienced by the sublattice. $H^i_{\rm eff}$ is the local effective field:

$$\boldsymbol{H}^i_{\rm eff} = K m_{i,x} \boldsymbol{e}_x - K_\perp m_{i,y} \boldsymbol{e}_y + A \partial_x^2 \boldsymbol{m}_i - J \boldsymbol{m}_{\bar{i}}, \tag{2}$$

where $\bar{i}$ stands for the opposite sublattice, that is $\bar{i} = B(A)$ for $i = A(B)$. The anisotropy easy (anisotropy constant K) and hard (anisotropy constant $K_\perp$) axes are taken along x and y directions, respectively. A is the intrasublattice exchange stiffness and J is the exchange coupling constant between the sublattices.

The torque $\boldsymbol{N}_i$ can be calculated starting from the effective exchange interaction between the spin densities on the two sides of the S/AF interface [58]:

$$H_{\rm int} = -\int d^2\boldsymbol{r} J_{\rm ex} \boldsymbol{S}_A \cdot \boldsymbol{s}, \tag{3}$$

where $\boldsymbol{s}$ is the electronic spin density operator in the S film, $\boldsymbol{S}_A$ is the localized spin operator in the AF film, belonging to the sublattice A. We assume that only the A sublattice is coupled to the interface, see Fig. 1. $J_{\rm ex}$ is the exchange constant and the integration is performed over the 2D interface. It has been shown [43] that this exchange interaction Hamiltonian results in the appearance of the exchange field $\boldsymbol{h}(\boldsymbol{r}) = -J_{\rm ex} M \boldsymbol{m}_A(\boldsymbol{r})/(2\gamma d_s)$ in the S film. The assumed interfacial interaction [Eq. (3)] conserves the total spin resulting in the general condition that spin lost by the superconductor appears as a spin torque exerted on the AF, as is derived rigorously below [Eq. (19)]. However, the presence of spin-orbit interaction at the interface can invalidate this relation and lead to

spin memory loss [61]. We disregard such effects here for simplicity. Furthermore, our $J_{\rm ex}$ is directly related to and can be expressed in terms of the spin mixing conductance parameter commonly used in a complementary scattering theory-based formulation of the spin torques [43,61–63].

Applying Ehrenfest's theorem from Eq. (3) one obtains the additional contribution to the Landau-Lifshitz-Gilbert equation written in the form of a torque acting on the magnetization:

$$\boldsymbol{N}_A = J_{\rm ex}\delta(z - z_I)\boldsymbol{m}_A(z) \times \langle \boldsymbol{s} \rangle, \quad \boldsymbol{N}_B = 0, \tag{4}$$

where the interface is located at $z = z_I$ and $\langle \boldsymbol{s} \rangle$ is the quantum mechanical averaged value of $\boldsymbol{s}$. Furthermore, we assume that the antiferromagnetic film is thin and its magnetization for a given sublattice is homogeneous in the z direction. In this case Eqs. (1) and (4) can be averaged over the thickness $d_{\rm AF}$ of the AF film. For the averaged torque we thus obtain

$$\overline{\boldsymbol{N}}_A = \frac{J_{\rm ex}\boldsymbol{m}_A \times \langle \boldsymbol{s} \rangle}{d_{\rm AF}}, \quad \overline{\boldsymbol{N}}_B = 0. \tag{5}$$

B. Microscopic calculation of the spin torque

In order to find the magnetization dynamics from Eq. (1), we need to calculate torque (5) microscopically by considering thermally induced quantum transport mediated by Cooper pairs and quasiparticles in the superconductor. The detailed calculation of the spin torque for a given effective exchange field in the superconductor can be found in Ref. [42] and is outlined below.

The superconductor is assumed to be in the ballistic limit. We neglect all the inelastic relaxation processes in the film assuming that its length is shorter than the corresponding relaxation length. As here we are dealing with the nonequilibrium problem, we work in the framework of the Keldysh technique for quasiclassical Green's functions. The matrix Green's function $\check{g}(\boldsymbol{r}, \boldsymbol{p}_F, \varepsilon, t)$ is an 8×8 matrix in the direct product of spin, particle-hole, and Keldysh spaces and depends on the spatial vector $\boldsymbol{r}$, quasiparticle momentum direction $\boldsymbol{p}_F$, quasiparticle energy ε, and time t. In the S film it obeys the Eilenberger equation:

$$i\boldsymbol{v}_F\nabla\check{g}(\boldsymbol{r}, \boldsymbol{p}_F) + [\varepsilon\tau_z + \boldsymbol{h}(\boldsymbol{r})\boldsymbol{\sigma}\tau_z - \check{\Delta}, \check{g}]_\otimes = 0, \tag{6}$$

where $[A, B]_\otimes = A \otimes B - B \otimes A$ and $A \otimes B = \exp[(i/2)(\partial_{\varepsilon_1}\partial_{t_2} - \partial_{\varepsilon_2}\partial_{t_1})]A(\varepsilon_1, t_1)B(\varepsilon_2, t_2)|_{\varepsilon_1=\varepsilon_2=\varepsilon; t_1=t_2=t}$. $\tau_{x,y,z}$ are Pauli matrices in particle-hole space with $\tau_\pm = (\tau_x \pm i\tau_y)/2$. $\hat{\Delta} = \Delta(x)\tau_+ - \Delta^*(x)\tau_-$ is the matrix structure of the superconducting order parameter $\Delta(x)$ in the particle-hole space.

In the ballistic limit treated here, it is convenient to use the so-called Riccati parametrization for the Green's function [64,65]. In terms of the Riccati parametrization the retarded Green's function takes the form

$$\check{g}^{R,A} = \pm N^{R,A} \otimes \begin{pmatrix} 1 - \hat{\Gamma}^{R,A} \otimes \hat{\tilde{\Gamma}}^{R,A} & 2\hat{\Gamma}^{R,A} \\ 2\hat{\tilde{\Gamma}}^{R,A} & -(1 - \hat{\tilde{\Gamma}}^{R,A} \otimes \hat{\Gamma}^{R,A}) \end{pmatrix}, \tag{7}$$

$$\check{g}^K = 2N^R \otimes \times \begin{pmatrix} x^K + \hat{\Gamma}^R \otimes \hat{\tilde{x}}^K \otimes \hat{\tilde{\Gamma}}^A & -(\hat{\Gamma}^R \otimes \hat{\tilde{x}}^K - \hat{x}^K\hat{\Gamma}^A) \\ \hat{\tilde{\Gamma}}^R \otimes \hat{x}^K - \hat{\tilde{x}}^K \otimes \hat{\tilde{\Gamma}}^A & \hat{\tilde{x}}^K + \hat{\tilde{\Gamma}}^R \otimes \hat{x}^K \otimes \hat{\Gamma}^A) \end{pmatrix} \otimes N^A, \tag{8}$$

with

$$N^{R,A} = \begin{pmatrix} 1 + \hat{\Gamma}^{R,A} \otimes \hat{\tilde{\Gamma}}^{R,A} & 0 \\ 0 & 1 + \hat{\tilde{\Gamma}}^{R,A} \otimes \hat{\Gamma}^{R,A} \end{pmatrix}^{-1}, \tag{9}$$

where $\hat{\Gamma}^{R,A}$, $\hat{\tilde{\Gamma}}^{R,A}$, $\hat{x}^K$, and $\hat{\tilde{x}}^K$ are matrices in spin space. Note that our parametrization differs from the definition in the literature [64,65] by factors $i\sigma_y$ as $\hat{\Gamma}^{R,A}_{\rm standard} = \hat{\Gamma}^{R,A} i\sigma_y$ and $\hat{\tilde{\Gamma}}^{R,A}_{\rm standard} = i\sigma_y\hat{\tilde{\Gamma}}^{R,A}$. The Riccati parametrization Eq. (7) obeys the normalization condition $\check{g} \otimes \check{g} = 1$ automatically.

The Riccati amplitude $\hat{\Gamma}$ obeys the following Riccati-type equations:

$$i\boldsymbol{v}_F\nabla\hat{\Gamma}^R + 2\varepsilon\hat{\Gamma}^R = -\hat{\Gamma}^R \otimes \Delta^* \otimes \hat{\Gamma}^R - \{\boldsymbol{h}\boldsymbol{\sigma}, \hat{\Gamma}^R\}_\otimes - \Delta \tag{10}$$

and $\hat{\tilde{\Gamma}}$ obeys the same equation with the substitution $\varepsilon \to -\varepsilon$, $\boldsymbol{h} \to -\boldsymbol{h}$, and $\Delta \to \Delta^*$.

The distribution function $\hat{x}^K$ obeys the equation

$$i\boldsymbol{v}_F\nabla\hat{x}^K + i\partial_t\hat{x}^K + \hat{\Gamma}^R \otimes \Delta^* \otimes \hat{x}^K + \hat{x}^K \otimes \Delta \otimes \hat{\tilde{\Gamma}}^A + [\boldsymbol{h}\boldsymbol{\sigma}, \hat{x}^K]_\otimes = 0, \tag{11}$$

while $\hat{\tilde{x}}^K$ obeys the same equation with the substitution $\boldsymbol{h} \to -\boldsymbol{h}$, $\Delta \to \Delta^*$, $\hat{\Gamma}^{R,A} \leftrightarrow \hat{\tilde{\Gamma}}^{R,A}$.

Considering a finite spatially inhomogeneous magnetic texture like a domain wall, the Riccati amplitudes $\hat{\Gamma}$ and $\hat{\tilde{\Gamma}}$ can be found from Eq. (10) numerically with the following asymptotic condition:

$$\begin{aligned} \hat{\Gamma}_\infty &= \Gamma_{0\infty} + \frac{\boldsymbol{h}_\infty\boldsymbol{\sigma}}{h}\Gamma_\infty, \\ \Gamma_{0\infty} &= -\frac{1}{2}\left[\frac{\Delta}{\varepsilon + h + i\sqrt{\Delta^2 - (\varepsilon + h)^2}} + \frac{\Delta}{\varepsilon - h + i\sqrt{\Delta^2 - (\varepsilon - h)^2}}\right], \\ \Gamma_\infty &= -\frac{1}{2}\left[\frac{\Delta}{\varepsilon + h + i\sqrt{\Delta^2 - (\varepsilon + h)^2}} - \frac{\Delta}{\varepsilon - h + i\sqrt{\Delta^2 - (\varepsilon - h)^2}}\right], \end{aligned} \tag{12}$$

and $\hat{\tilde{\Gamma}}_\infty = -\hat{\Gamma}_\infty$. In Eqs. (12) $h = |\boldsymbol{h}|$ is the absolute value of the effective exchange field, which is spatially constant. ε has an infinitesimal imaginary part δ, where δ is positive for the retarded functions.

Equation (10) is numerically stable if it is solved starting from $x = -\infty$ for right-going trajectories $v_x > 0$ and from $x = +\infty$ for left-going trajectories $v_x < 0$. On the contrary, $\hat{\tilde{\Gamma}}$ can be found numerically starting from $x = +\infty$ for right-going trajectories $v_x > 0$ and from $x = -\infty$ for left-going trajectories $v_x < 0$. The advanced Riccati amplitudes can be found taking into account the relation [65] $\hat{\Gamma}^A = -(\hat{\tilde{\Gamma}}^R)^\dagger$.

If we neglect the dependence of $\boldsymbol{h}$ on time, then it follows from Eq. (11) that the distribution function $\hat{x}^K$ for a given ballistic trajectory is determined by the equilibrium distribution function of the left (right) reservoir for $v_{F,x} > 0$ ($v_{F,x} < 0$) and takes the form

$$\hat{x}^K_{\pm} = (1 + \hat{\gamma}^R_{\pm} \otimes \hat{\tilde{\gamma}}^A_{\pm}) \tanh \frac{\varepsilon}{2T_{l,r}}, \tag{13}$$

where the subscript $+$ $(-)$ corresponds to the trajectories $v_{F,x} > 0$ ($v_{F,x} < 0$). On the contrary,

$$\hat{\tilde{x}}^K_{\pm} = -(1 + \hat{\tilde{\gamma}}^R_{\pm} \otimes \hat{\gamma}^A_{\pm}) \tanh \frac{\varepsilon}{2T_{r,l}}. \tag{14}$$

The terms $\propto \dot{\boldsymbol{h}}$ in Eq. (11) can be neglected under the condition $(h/\Delta)v_{\rm st}/l_{\rm DW}\Delta \ll 1$, where $v_{\rm st}$ is the velocity of the rigid DW motion caused by the thermal gradient under consideration, and $l_{\rm DW}$ is the DW width. For realistic parameters $v_{\rm st} \sim 100$ m/s according to our estimates below. Therefore, at $\Delta \sim 1K$ and $h/\Delta \lesssim 1$ these conditions are fulfilled to a good accuracy for any experimentally reasonable DW width $l_{\rm DW} \sim 10$ nm–1 μm.

The superconducting order parameter is found self-consistently according to

$$\Delta = -\frac{\lambda}{8} \int_{-\Omega}^{\Omega} d\varepsilon \mathrm{Tr}_4 \langle \tau_- \check{g}^K \rangle, \tag{15}$$

where $\langle \cdots \rangle$ denotes averaging over the Fermi surface, λ is the coupling constant, and Ω is the Debye frequency cutoff. The spatial dependence of the superconducting order parameter due to the localized domain wall is found to be weak [42]. On the other hand, the suppression of the order parameter due to finite temperature and exchange field in the superconductor is relatively important. Therefore, in the present study we only account for the spatially uniform temperature and exchange field-induced suppression of superconductivity neglecting the tiny spatial effects near the DW. In this case the order parameter can be calculated using the bulk expressions for the Riccati amplitudes Eqs. (12). Substituting the Riccati amplitudes and the distribution functions (13) and (14) into the self-consistency equation (15) we finally end up with

$$\Delta = -\frac{\lambda}{4} \int_0^{\Omega} d\varepsilon \mathrm{Re} \left[\frac{i\Delta}{\sqrt{\Delta^2 - (\varepsilon + i\delta + h)^2}} + \frac{i\Delta}{\sqrt{\Delta^2 - (\varepsilon + i\delta - h)^2}} \right] \left(\tanh \frac{\varepsilon}{2T_l} + \tanh \frac{\varepsilon}{2T_r} \right). \tag{16}$$

From Eq. (6) it can be shown that $\langle \boldsymbol{s} \rangle$ obeys the following equation:

$$\partial_t \langle \boldsymbol{s} \rangle = -\partial_j \boldsymbol{J}_j - 2\boldsymbol{h} \times \langle \boldsymbol{s} \rangle, \tag{17}$$

where we have introduced vector $\boldsymbol{J}_j = (J^x_j, J^y_j, J^z_j)$ corresponding to the spin current flowing along the j axis in the coordinate space:

$$\boldsymbol{J}_j = -\frac{N_F}{16} \int_{-\infty}^{\infty} d\varepsilon \mathrm{Tr}_4 [\boldsymbol{\sigma} \langle v_{F,j} \check{g}^K \rangle], \tag{18}$$

where N_F is the normal state density of states at the Fermi level and v_F is the Fermi velocity.

Considering the steady state of the conduction electrons, Eq. (17) yields

$$\overline{\boldsymbol{N}}_A = \frac{\gamma d_S}{M d_{\rm AF}} \partial_j \boldsymbol{J}_j. \tag{19}$$

III. RESULTS

A. Numerical evaluation of thermally induced DW motion

Now we present the results of numerical simulations of the magnetization dynamics in the AF based on LLG Eqs. (1). The spin torque exerted by the superconductor is calculated microscopically according to Eqs. (18) and (19). The Néel vector in the AF $\boldsymbol{n} = (\boldsymbol{m}_A - \boldsymbol{m}_B)/2$ can be parametrized as

$$\boldsymbol{n} = (\cos\theta, \sin\theta \sin\phi, \sin\theta \cos\phi), \tag{20}$$

where both angles θ and ϕ depend on the x coordinate. The equilibrium shape of the DW in the absence of the superconducting film is given by $\cos\theta = \tanh(x/d_{\rm DW})$ and $\phi = 0$, that is the DW is in the x-z plane.

For the numerical calculation we introduce the dimensionless quantities $\tilde{t} = t(\gamma K)$ and $\tilde{\boldsymbol{H}}_{\rm eff} = m_{i,x}\boldsymbol{e}_x - k m_{i,y}\boldsymbol{e}_y + \tilde{A}\partial^2_x \boldsymbol{m}_i - \tilde{J}\boldsymbol{m}_{\tilde{i}}$ with $\tilde{A} = A/K$, $\tilde{J} = J/K$, $k = K_\perp/K$. All lengths are measured in units of $\xi_S = v_F/\Delta_0$, $\tilde{x} = x/\xi_S$. Here Δ_0 is the superconducting order parameter of the S film in the absence of the antiferromagnet at $T = 0$. The dimensionless torque is $\tilde{\boldsymbol{N}}_A = \overline{\boldsymbol{N}}_A/\gamma K = \zeta \partial_{\tilde{x}} \tilde{\boldsymbol{J}}_x$, where the dimensionless quantity $\partial_{\tilde{x}} \tilde{\boldsymbol{J}}_x = (2e^2 R_N v_F/\Delta_0^2)\partial_x \boldsymbol{J}_x$ and $\zeta = E_S/\pi E_A$ is proportional to the ratio of the condensation energy $E_S = N_F \Delta_0^2 d_S/2$ and the anisotropy energy $E_A = MKd_{\rm AF}/2$. Here and below $R_N = \pi/(2e^2 N_F v_F)$ is the normal state resistance of the S film. For estimates we take $E_S \sim (10\text{–}10^3) \times d_S$ erg/sm^2 (for conventional superconductors like Al and Nb) and assume that characteristic values of E_A for antiferromagnets are close to the corresponding values for ferromagnets: $E_A \sim 10^5 d$ erg/sm^2 for Py thin films [66] or $E_A \sim (10\text{–}10^2) \times d$ erg/sm^2 for YIG thin films [67]. This implies that ζ can vary in wide range $\zeta \sim (10^{-4}\text{–}10^2)(d_S/d_{\rm AF})$. For our numerical analysis we assume $\zeta = 0.048$.

Figure 2 depicts snapshots of the spatial profiles of the Néel vector $\boldsymbol{n}$ at several subsequent moments during the DW motion under the applied temperature difference for the finite value of the hard-axis anisotropy $k = 1$. It is seen that the DW moves as a rigid object preserving its initial shape, that is the motion is in the regime well below the Walker breakdown [4]. The motion is in this regime for the entire temperature range where the superconductivity survives.

In Fig. 3 we plot the velocity of the moving DW as a function of the left (hot) end temperature T_l. The velocity is measured in units of $v_0 = \xi_S/t_0$, where $t_0 = (\gamma K)^{-1}$. Taking typical values of the superconducting Al coherence length $\xi_S \sim 200$ nm and $K \sim 10^2$ G we can roughly estimate $v_0 \sim 10^4\text{–}10^5$ cm/s. Figure 3(a) demonstrates the DW velocity for nearly zero temperature of the right end of the bilayer $T_r = 0.02\Delta_0$. It is seen that the velocity becomes finite even at $T_l > T_{c0} \approx 0.57\Delta_0$, where T_{c0} is the critical temperature of the superconductor in the absence of the antiferromagnet. This implies that the superconductivity still survives at such temperature differences. This existence of superconductivity at large temperatures is a specific feature of the ballistic

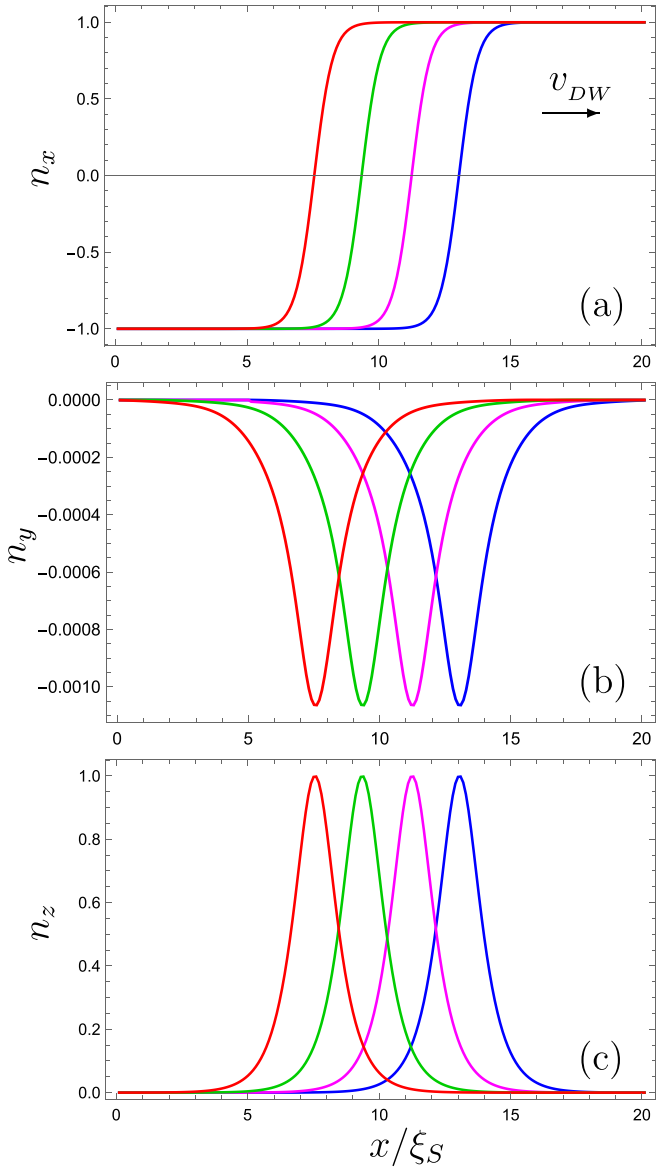

FIG. 2. Spatial profiles of the Néel vector at several subsequent times. $T_l = 0.32\Delta_0$, $T_r = 0.02\Delta_0$, $d = \xi_S$, $\alpha = 0.01$, $\alpha_c = 0.009$, $h = 0.3\Delta_0$, the time between two subsequent curves $dt = 10t_0$. The DW moves from the left (hot) to the right (cold) end. The direction of the DW motion is indicated by the arrow in (a).

limit, which results from the fact that at a given point only a half of all the trajectories, corresponding to $v_x > 0$ carry hot quasiparticles distributed in accordance with T_l. The other half of trajectories $v_x < 0$ carry no quasiparticles because they are not produced at the right end at $T = 0$. Mathematically these arguments are expressed by Eq. (16), where the order parameter is determined by the sum of two Fermi functions, corresponding to the both ends of the bilayer.

At the same time Fig. 3(b) corresponds to $T_r = 0.32\Delta_0$. At this value of the cold end temperature the amount of left-moving quasiparticles from the right (cold) end is enough to completely suppress superconductivity already at $T_l = 0.82\Delta_0$. As a result the DW velocity goes to zero at this temperature.

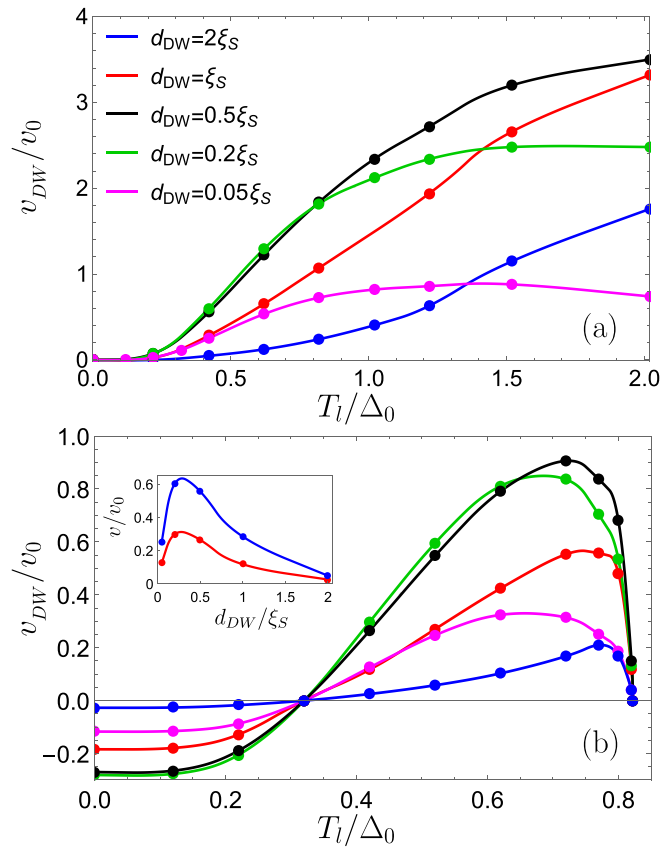

FIG. 3. (a) DW velocity as a function of T_l at $T_r = 0.02\Delta_0$ for different DW widths. (b) DW velocity as a function of T_l at $T_r = 0.32\Delta_0$ for different DW widths. The inset shows the DW velocity at $T_l = 0.42\Delta_0$ and $T_r = 0.32\Delta_0$ (red) or $T_r = 0$ (blue) as a function of the DW width. The parameters α, α_c, and h are the same as in Fig. 2.

Different curves in Fig. 3 correspond to different values of the DW width $d_{\rm DW}$ in units of ξ_S. It is seen that for a given temperature difference the DW velocity is a nonmonotonic function of $d_{\rm DW}$ exhibiting a maximum at $d_{\rm DW} \sim \xi_S/3$. The dependence of the DW velocity as a function of $d_{\rm DW}$ is demonstrated in the inset of Fig. 3(b). This can be understood via the argument that the DW motion is driven by the nonadiabatic torque component, which is $\propto d_{\rm DW}/\xi_S$ at small values of this parameter (see analytical calculations below). Furthermore, the spin torque vanishes at large $d_{\rm DW} \gg \xi_S$ because the electron spin can trace the magnetization in this case and the nonadiabatic torque goes to zero. Thus, the spin torque exerted is bound to achieve a maximum value in between the two extremes where it vanishes.

B. Analytical calculation of the DW velocity in the framework of the collective coordinates approach

In the present section we employ the collective coordinates approach for AFs [17] in obtaining analytic results for the DW velocity. Furthermore, in the limit of a narrow DW, the thermally generated spin current in S is also evaluated analytically.

We substitute $\boldsymbol{m}_{A,B} = \boldsymbol{m} \pm \boldsymbol{n}$ into Eq. (1) and after some algebra obtain

$$\frac{\partial \boldsymbol{n}}{\partial t} = -\gamma[\boldsymbol{n} \times \boldsymbol{H}^m + \boldsymbol{m} \times \boldsymbol{H}^n] + \frac{\overline{\boldsymbol{N}}_A}{2} + \alpha_n \boldsymbol{n} \times \frac{\partial \boldsymbol{m}}{\partial t} + \alpha_m \boldsymbol{m} \times \frac{\partial \boldsymbol{n}}{\partial t}, \tag{21}$$

$$\frac{\partial \boldsymbol{m}}{\partial t} = -\gamma[\boldsymbol{n} \times \boldsymbol{H}^n + \boldsymbol{m} \times \boldsymbol{H}^m] + \frac{\overline{\boldsymbol{N}}_A}{2} + \alpha_m \boldsymbol{m} \times \frac{\partial \boldsymbol{m}}{\partial t} + \alpha_n \boldsymbol{n} \times \frac{\partial \boldsymbol{n}}{\partial t}, \tag{22}$$

where $\boldsymbol{H}^{m,n} = (\boldsymbol{H}^A_{\text{eff}} \pm \boldsymbol{H}^B_{\text{eff}})/2$ and $\alpha_{m,n} = \alpha \pm \alpha_c$. We further take into account that $m \ll 1$. Then multiplying Eq. (21) by $\times \boldsymbol{n}$ and accounting for $n^2 \approx 1$ and $\boldsymbol{n} \cdot \boldsymbol{m} = 0$, we obtain the leading order expression for $\boldsymbol{m}$:

$$\boldsymbol{m} = \frac{1}{2\gamma J}\left[\partial_t \boldsymbol{n} \times \boldsymbol{n} + \boldsymbol{n} \times \frac{\overline{\boldsymbol{N}}_A}{2}\right], \tag{23}$$

where we have also neglected small terms $\sim \alpha_{m,n}$ and $\alpha^2_{m,n}$. Equation (23) is quite standard [12] except for the fact that the torque term, in our case, stems only from one of the sublattices.

When magnetic textures are rigid, only a few soft modes dominate the magnetization dynamics. In this case the evolution of the soft modes can be described by a finite set of collective coordinates. This method was successfully applied both for ferromagnetic [4,68,69] and antiferromagnetic [17] textures. Our numerical results presented in Fig. 2 demonstrate that the magnetization texture for the problem under consideration is rigid and, therefore, we exploit the collective coordinate method to analytically describe the DW motion. We use the DW center coordinate x_{DW} and the out-of-plane tilt angle ϕ as collective coordinates. In this case the Néel vector of the moving DW can be written in the form of Eq. (20) with $\theta = \theta[x - x_{\text{DW}}(t)]$ and $\phi = \phi(t)$. Substituting Eq. (23) into Eq. (22) and keeping in Eq. (22) only terms up to the linear order with respect to $\overline{\boldsymbol{N}}_A$ and $\dot{x}_{\text{DW}} \sim \overline{\boldsymbol{N}}_A$, we obtain

$$\frac{\boldsymbol{n} \times \ddot{\boldsymbol{n}}}{2\gamma J} - \gamma \boldsymbol{n} \times \boldsymbol{H}^n + \alpha_n \boldsymbol{n} \times \dot{\boldsymbol{n}} + \frac{\overline{\boldsymbol{N}}_A}{2} = 0. \tag{24}$$

By projecting this equation on the y axis and substituting the Néel vector in the form (20) we get

$$\frac{\theta' \ddot{x}_{\text{DW}}}{2\gamma J} + \alpha_n \theta' \dot{x}_{\text{DW}} + \frac{\overline{N}^{\text{ne}}_{A,y}}{2} = 0, \tag{25}$$

where θ' is the derivative of θ with respect to its argument and $\overline{N}^{\text{ne}}_{A,y} = \overline{N}_{A,y} - \overline{N}^{\text{eq}}_{A,y}$ is the nonequilibrium part of the torque, which arises due to applied temperature difference. The equilibrium contribution $\overline{N}^{\text{eq}}_{A,y}$ exists also at $\Delta T = 0$ and is compensated by a small distortion of the DW shape in S/AF bilayer with respect to the isolated AF film [42]. By multiplying Eq. (25) by θ' and integrating over x coordinate it can be represented in the form of equation of motion [17] for the collective coordinate x_{DW} with the effective mass of the DW $M = (1/J\gamma^2)\int(\theta')^2 dx$ and the total force inducing the DW motion $F = -(1/\gamma)\int \overline{N}^{\text{ne}}_{A,y}\theta' dx$.

Furthermore, we consider the regime of a steady-state motion of the DW and in this case $\phi(t) = \phi_0$ and the massive term in Eq. (25) is zero. This equation is strictly valid only for the special shape of the torque $\overline{N}^{\text{ne}}_{A,y} \propto \theta'$, which coincides with the phenomenological expression for nonadiabatic torque considered in Ref. [17]. Our microscopic numerical calculations indicate that this condition is approximately valid at $|x - x_{\text{DW}}| < x_0$, where $x_0 \lesssim \xi_S$. Therefore, the DW velocity can be approximately found as

$$v_{\text{DW}} = \dot{x}_{\text{DW}} = \frac{\overline{N}^0_{A,y} d_{\text{DW}}}{2\alpha_n}, \tag{26}$$

where $\overline{N}^0_{A,y} = \overline{N}_{A,y}(x = x_{\text{DW}})$. A slightly more accurate result taking into account the averaging over the DW region can be obtained by integrating Eq. (25):

$$v_{\text{DW}} = \frac{\int_{-x_0}^{x_0} \overline{N}_{A,y} dx}{2\alpha_n[\theta(x_0) - \theta(-x_0)]}. \tag{27}$$

This integrated expression is not very useful for analytical calculation of the DW velocity in case $d_{\text{DW}} > \xi_S$ because the parameter x_0 can only be extracted from numerical calculations. At the same time here we focus on the regime $d_{\text{DW}} \ll \xi_S$, which is relevant for Al-based AF/S bilayers due to the relatively large coherence length ξ_S in Al. In this regime the main part of the integral in Eq. (27) comes from the region $|x - x_{\text{DW}}| < d_{\text{DW}}$ and, therefore, the exact value of $x_0 \gg d_{\text{DW}}$ is not important.

Analogously, by taking a projection of Eq. (24) on the x axis one can find the tilt angle

$$\phi_0 = \frac{\int_{-x_0}^{x_0} \overline{N}_{A,x} dx}{4 d_{\text{DW}} \gamma K_\perp}. \tag{28}$$

Comparing this result to the tilt angle for the ferromagnetic case

$$\phi_F = \frac{1}{\gamma K_\perp d_{\text{DW}}}\left[\frac{1}{2}\int_{-x_0}^{x_0} dx N_x - \frac{1}{\pi\alpha}\int_{-x_0}^{x_0} dx N_z\right], \tag{29}$$

we see that due to the absence of the last term $\propto \alpha^{-1} \gg 1$ in Eq. (28) the tilt angle in antiferromagnets is much smaller than in ferromagnets and can be considered as a hard mode, as it has been indicated in Ref. [17]. It is a manifestation of the qualitatively different behavior of magnetization dynamics in ferromagnets and antiferromagnets.

The DW velocity v_{DW} is $\propto \alpha_n^{-1}$ in agreement with our numerical analysis (see Fig. 4). It is also $\propto \int_{-x_0}^{x_0} \overline{N}_{A,y} dx$. For a plane DW under consideration the latter quantity is nothing but the nonadiabatic torque, integrated over the coordinate. Contrary to the phenomenological approaches, which were applied before to study DW motion in ferromagnetic and antiferromagnetic textures, we calculate the nonadiabatic torque microscopically. It is done numerically for a wide range of parameters and the resulting DW motion has been discussed in the previous section.

In the regime $d_{\text{DW}} \ll \xi_S$ we are able to obtain an approximate analytical expression for the integrated nonadiabatic torque. According to Eq. (19) $\int_{-x_0}^{x_0} \overline{N}_{A,y} dx \propto \int_{-x_0}^{x_0} d\boldsymbol{J}_y/dx = \boldsymbol{J}_y(x_0) - \boldsymbol{J}_y(-x_0)$. The last difference is mainly determined by the jump of the y component of the spin current $\Delta \boldsymbol{J}_y$ at the

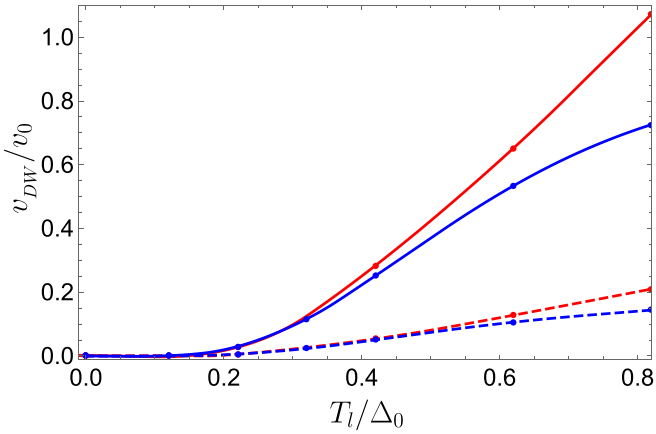

FIG. 4. Numerically calculated DW velocity as a function of T_l at different DW widths $d_{\rm DW} = \xi_S$ (red) and $d_{\rm DW} = 0.05\xi_S$ (blue) and different values of $\alpha_n = 0.001$ (solid) and $\alpha_n = 0.005$ (dashed). $T_r = 0.02\Delta_0$. It is seen that the DW velocity is proportional to α_n^{-1} for any widths of the DW.

DW. This jump can be found analytically in the framework of the perturbation theory with respect to the small parameter $d_{\rm DW}/\xi_S \ll 1$. In this regime the DW can be viewed as very narrow as compared to the superconducting coherence length and we can find the solution of Eq. (10) at the left and right boundaries of the DW, that is at $x = \mp d_{\rm DW} \approx 0$, where the zero-order contribution is continuous, while the first order contribution to the Riccati amplitudes exhibits a jump:

$$\hat\Gamma^R_+(-d_{\rm DW}) = \hat\Gamma^R_{l,-\infty}, \quad \hat\Gamma^R_+(d_{\rm DW}) = \hat\Gamma^R_{l,-\infty} + \delta\Gamma\hat\sigma_z, \quad (30)$$

$$\hat\Gamma^R_-(d_{\rm DW}) = \hat\Gamma^R_{r,+\infty}, \quad \hat\Gamma^R_-(-d_{\rm DW}) = \hat\Gamma^R_{r,+\infty} + \delta\Gamma\hat\sigma_z, \quad (31)$$

$$\hat{\tilde\Gamma}^R_+(d_{\rm DW}) = -\hat\Gamma^R_{r,+\infty}, \quad \hat{\tilde\Gamma}^R_+(-d_{\rm DW}) = -\hat\Gamma^R_{r,+\infty} - \delta\Gamma\hat\sigma_z, \quad (32)$$

$$\hat{\tilde\Gamma}^R_-(-d_{\rm DW}) = -\hat\Gamma^R_{l,-\infty}, \quad \hat{\tilde\Gamma}^R_-(d_{\rm DW}) = -\hat\Gamma^R_{l,-\infty} - \delta\Gamma\hat\sigma_z, \quad (33)$$

where

$$\delta\Gamma = \int_{-\infty}^{+\infty} h_z(x)\mathrm{Tr}[\hat\Gamma^{R,0}(x)]dx, \quad (34)$$

where due to the condition $d_{\rm DW}/\xi_S \ll 1$ the zero order contribution to the Riccati-amplitudes $\hat\Gamma^{R,0}(x)$ can be taken at $x = 0$: $\hat\Gamma^{R,0}_\pm(x) \approx \Gamma^{R,0}_\pm(0) = \hat\Gamma^R_{l(r),\infty}$. Accounting for this approximation the first-order contribution to the Riccati amplitudes takes the form

$$\delta\Gamma = \frac{2\pi d_{\rm DW} h}{i|v_{F,x}|}\Gamma_{0\infty}. \quad (35)$$

Composing the Green's function from the Riccati amplitudes and substituting it into Eq. (18) we end up with the following result:

$$\Delta\boldsymbol{J}_y = \frac{\pi N_F d_{\rm DW} h}{2}\int_{-\infty}^{\infty} d\varepsilon \frac{|I_1|^2 - |I_2|^2}{|I_1 I_2 - 1|^2} \times\left[\tanh\left(\frac{\varepsilon}{2T_l}\right) - \tanh\left(\frac{\varepsilon}{2T_r}\right)\right], \quad (36)$$

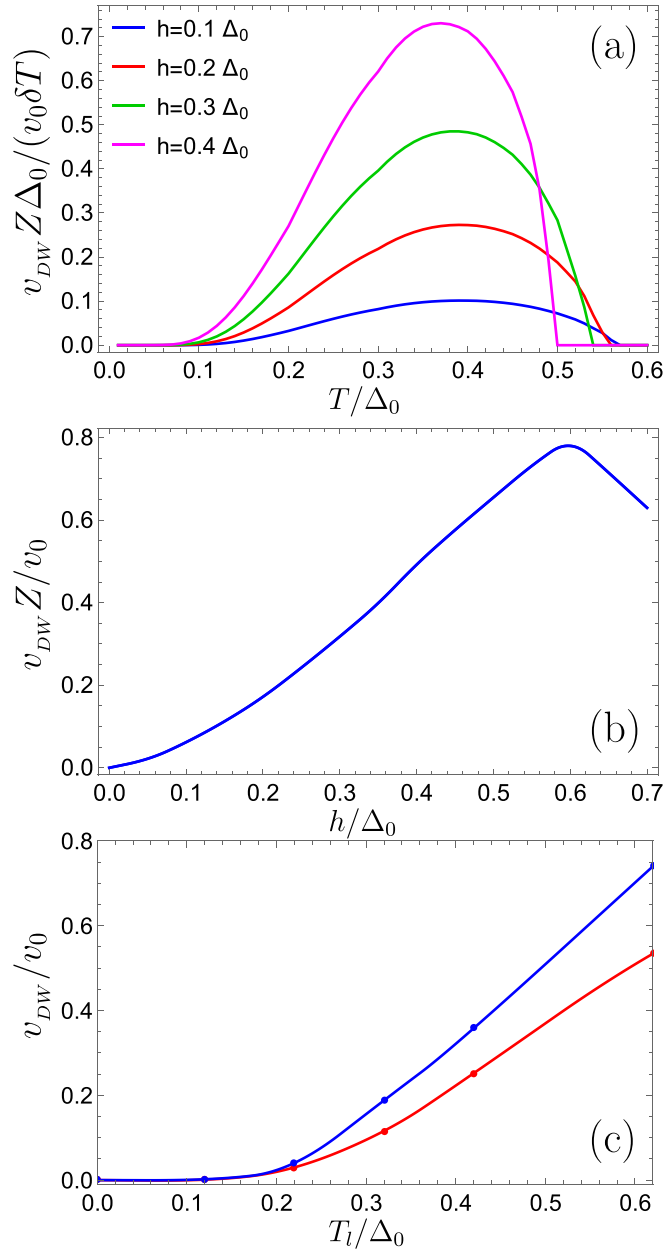

FIG. 5. (a) $v_{\rm DW}$ as a function of T at small temperature differences $\delta T = T_l - T_r \ll T$ calculated according to the analytical expression Eq. (38). (b) Maximal $v_{\rm DW}$ for a given h, which can be reached by properly adjusting the temperature difference $T_l - T_r$. (c) Comparison of the numerical (red) and analytical (blue) results for the DW velocity as a function of T_l. The cold end temperature $T_r = 0.02\Delta_0$, $d_{\rm DW} = 0.05\xi_S$, $\alpha = 0.01$, $\alpha_c = 0.009$.

where

$$I_{1,2} = \frac{\varepsilon + i\delta \pm h + i\sqrt{\Delta^2 - (\varepsilon + i\delta \pm h)2}}{\Delta}. \quad (37)$$

Substituting this expression for $\Delta\boldsymbol{J}_y$ into Eq. (27) we finally obtain the following analytical expression for the DW velocity

valid at $d_{\mathrm{DW}} \ll \xi_S$:

$$v_{\mathrm{DW}} = Z^{-1} v_0 \frac{h}{\Delta_0} \int_{-\infty}^{\infty} \frac{d\varepsilon}{\Delta_0} \frac{|I_1|^2 - |I_2|^2}{|I_1 I_2 - 1|^2} \times \left[\tanh\left(\frac{\varepsilon}{2T_l}\right) - \tanh\left(\frac{\varepsilon}{2T_r}\right) \right], \tag{38}$$

where $Z = 8\alpha_n \xi_S/(\pi \zeta d_{\mathrm{DW}})$ is the parameter containing the dependence of the DW velocity on all the essential quantities, such as ζ, α_n, and d_{DW}, except for the dependence on the exchange field h.

The DW velocity calculated according to Eq. (38) at small temperature differences $\delta T = T_l - T_r \ll T$ is shown in Fig. 5(a) for different values of the exchange field h. It is seen that in general v_{DW} is higher for larger values of h, but it also more sharply vanishes at high temperatures because of the superconductivity suppression by the exchange field. Figure 5(b) demonstrates the maximum value of v_{DW}, which can be obtained for a given h by properly adjusting the temperature difference $T_l - T_r$, calculated according to Eq. (38). The maximal value of the DW velocity grows with the exchange field until the superconductivity suppression by h becomes strong enough and dominates in the dependence of v_{DW} on the exchange field.

Equation (38) can be further simplified at not very small values of the exchange field $0.1\Delta \lesssim h \lesssim \Delta$. In this case the integrand in Eq. (36) can be approximated as

$$\frac{|I_1|^2 - |I_2|^2}{|I_1 I_2 - 1|^2} \approx \frac{\operatorname{sgn}\varepsilon}{4} \left(1 + \frac{2\Delta}{h}\right) \sqrt{\varepsilon^2 - (\Delta - h)^2} \tag{39}$$

if $\varepsilon \in \pm[\Delta - h, \Delta + h]$ and it is zero beyond this energy interval. With this approximation

$$v_{\mathrm{DW}} = Z^{-1} v_0 \frac{h}{\Delta_0} [F(h, T_l) - F(h, T_r)],$$
$$F(h, T) = \left(1 + \frac{2\Delta}{h}\right) \sqrt{\frac{2(\Delta - h)}{\Delta_0}} \frac{T}{\Delta_0} e^{-\frac{\Delta - h}{T}} \times \left(\frac{\sqrt{\pi}}{2} - \sqrt{\frac{2h}{T}} e^{-\frac{2h}{T}} \right). \tag{40}$$

Equation (40) can be further simplified at $T_{l,r} \ll \Delta$ resulting in

$$v_{\mathrm{DW}} = \frac{\sqrt{\pi}}{2} Z^{-1} v_0 \frac{h}{\Delta_0} \left(1 + \frac{2\Delta}{h}\right) \sqrt{\frac{2(\Delta - h)}{\Delta_0}} \times \left(T_l e^{-\frac{\Delta - h}{T_l}} - T_r e^{-\frac{\Delta - h}{T_r}} \right). \tag{41}$$

Expressions (40) and (41) reflect the main qualitative features observed in the exact numerical results presented in Fig. 3. In particular, v_{DW} is exponentially suppressed at low temperatures $T_{l,r} \ll (\Delta - h)$, as it is seen in Fig. 3(a) and can be qualitatively explained by the fact that the number of quasiparticles contributing to the giant thermospin effect is exponentially suppressed at such low temperatures. At moderate temperatures $T > (\Delta - h)$ the DW velocity is roughly proportional to $T_l - T_r$, which is also seen from the numerical results. This behavior is changed by the velocity reduction upon further increase of temperature when the suppression of the superconducting gap by temperature becomes essential.

IV. CONCLUSIONS

A high-efficiency thermally induced 180° antiferromagnetic domain-wall (DW) motion is predicted in thin-film AF/S hybrid structures with uncompensated magnetization at the AF/S interface. The surface magnetization gives rise to an effective exchange field and a spin splitting of the DOS in the superconductor. The physical mechanism underlying the torque hat drives DW motion is connected to the generation of the giant spin-dependent Seebeck effect in the spin-split superconductor, which pumps quasiparticle spin into the superconducting region in the vicinity of the DW. The resulting DW motion is investigated both numerically and analytically. The analyzed dependence of the DW velocity on the effective exchange field, Gilbert damping, and the DW width offers valuable guidance for the experimental realization and optimization of the suggested mechanism. We estimate relatively high DW velocities ~100 m/s at small temperature differences ~1 K applied across a length equivalent to several domain-wall widths.

ACKNOWLEDGMENTS

The work of I.V.B. and A.M.B. was supported by RSF project 21-12-00185. I.V.B. also acknowledges the financial support by Foundation for the Advancement of Theoretical Physics and Mathematics "BASIS." A.K. acknowledges financial support from the Research Council of Norway through its Centers of Excellence funding scheme, project 262633, "QuSpin."

[1] B. Göbel, I. Mertig, and O. A. Tretiakov, Beyond skyrmions: Review and perspectives of alternative magnetic quasiparticles, Phys. Rep. **895**, 1 (2020).

[2] H. Yu, J. Xiao, and H. Schultheiss, Magnetic texture based magnonics, arXiv:2010.09180.

[3] J. Han, P. Zhang, J. T. Hou, S. A. Siddiqui, and L. Liu, Mutual control of coherent spin waves and magnetic domain walls in a magnonic device, Science **366**, 1121 (2019).

[4] N. L. Schryer and L. R. Walker, The motion of 180° domain walls in uniform dc magnetic fields, J. Appl. Phys. **45**, 5406 (1974).

[5] D. C. Ralph and M. D. Stiles, Spin transfer torques, J. Magn. Magn. Mater. **320**, 1190 (2008).

[6] S. U. Jen and L. Berger, Thermal domain drag effect in amorphous ferromagnetic materials. II. Experiments, J. Appl. Phys. **59**, 1285 (1986).

[7] W. Jiang, P. Upadhyaya, Y. Fan, J. Zhao, M. Wang, L.-T. Chang, M. Lang, K. L. Wong, M. Lewis, Y.-T. Lin, J. Tang, S. Cherepov, X. Zhou, Y. Tserkovnyak, R. N. Schwartz, and K. L. Wang, Direct Imaging of Thermally Driven Domain Wall Motion in Magnetic Insulators, Phys. Rev. Lett. **110**, 177202 (2013).

[8] G. E. W. Bauer, E. Saitoh, and B. J. van Wees, Spin caloritronics, Nat. Mater. **11**, 391 (2012).

[9] M. Hatami, G. E. W. Bauer, Q. Zhang, and P. J. Kelly, Thermal Spin-Transfer Torque in Magnetoelectronic Devices, Phys. Rev. Lett. **99**, 066603 (2007).

[10] D. Hinzke and U. Nowak, Domain Wall Motion by the Magnonic Spin Seebeck Effect, Phys. Rev. Lett. **107**, 027205 (2011).

[11] J. C. Slonczewski, Initiation of spin-transfer torque by thermal transport from magnons, Phys. Rev. B **82**, 054403 (2010).

[12] E. V. Gomonay and V. M. Loktev, Spintronics of antiferromagnetic systems (review article), Low Temp. Phys. **40**, 17 (2014).

[13] V. Baltz, A. Manchon, M. Tsoi, T. Moriyama, T. Ono, and Y. Tserkovnyak, Antiferromagnetic spintronics, Rev. Mod. Phys. **90**, 015005 (2018).

[14] T. Jungwirth, J. Sinova, A. Manchon, X. Marti, J. Wunderlich, and C. Felser, The multiple directions of antiferromagnetic spintronics, Nat. Phys. **14**, 200 (2018).

[15] T. Jungwirth, X. Marti, P. Wadley, and J. Wunderlich, Antiferromagnetic spintronics, Nat. Nanotechnol. **11**, 231 (2016).

[16] H. V. Gomonay and V. M. Loktev, Spin transfer and current-induced switching in antiferromagnets, Phys. Rev. B **81**, 144427 (2010).

[17] E. G. Tveten, A. Qaiumzadeh, O. A. Tretiakov, and A. Brataas, Staggered Dynamics in Antiferromagnets by Collective Coordinates, Phys. Rev. Lett. **110**, 127208 (2013).

[18] H. Y. Yuan, Z. Yuan, R. A. Duine, and X. R. Wang, Recent progress in antiferromagnetic dynamics, EPL **132**, 57001 (2020).

[19] K.-J. Kim, S. K. Kim, Y. Hirata, S.-H. Oh, T. Tono, D.-H. Kim, T. Okuno, W. S. Ham, S. Kim, G. Go, Y. Tserkovnyak, A. Tsukamoto, T. Moriyama, K.-J. Lee, and T. Ono, Fast domain wall motion in the vicinity of the angular momentum compensation temperature of ferrimagnets, Nat. Mater. **16**, 1187 (2017).

[20] K. Uchida, J. Xiao, H. Adachi, J. Ohe, S. Takahashi, J. Ieda, T. Ota, Y. Kajiwara, H. Umezawa, H. Kawai, G. E. W. Bauer, S. Maekawa, and E. Saitoh, Spin Seebeck insulator, Nat. Mater. **9**, 894 (2010).

[21] S. Meyer, Y.-T. Chen, S. Wimmer, M. Althammer, T. Wimmer, R. Schlitz, S. Geprägs, H. Huebl, D. Ködderitzsch, H. Ebert, G. E. W. Bauer, R. Gross, and S. T. B. Goennenwein, Observation of the spin Nernst effect, Nat. Mater. **16**, 977 (2017).

[22] O. Gomonay, K. Yamamoto, and J. Sinova, Spin caloric effects in antiferromagnets assisted by an external spin current, J. Phys. D **51**, 264004 (2018).

[23] P. Yan, X. S. Wang, and X. R. Wang, All-Magnonic Spin-Transfer Torque and Domain Wall Propagation, Phys. Rev. Lett. **107**, 177207 (2011).

[24] X. S. Wang and X. R. Wang, Thermodynamic theory for thermal-gradient-driven domain-wall motion, Phys. Rev. B **90**, 014414 (2014).

[25] F. Schlickeiser, U. Ritzmann, D. Hinzke, and U. Nowak, Role of Entropy in Domain Wall Motion in Thermal Gradients, Phys. Rev. Lett. **113**, 097201 (2014).

[26] S. Selzer, U. Atxitia, U. Ritzmann, D. Hinzke, and U. Nowak, Inertia-Free Thermally Driven Domain-Wall Motion in Antiferromagnets, Phys. Rev. Lett. **117**, 107201 (2016).

[27] A. Donges, N. Grimm, F. Jakobs, S. Selzer, U. Ritzmann, U. Atxitia, and U. Nowak, Unveiling domain wall dynamics of ferrimagnets in thermal magnon currents: Competition of angular momentum transfer and entropic torque, Phys. Rev. Res. **2**, 013293 (2020).

[28] P. Yan, A. Kamra, Y. Cao, and G. E. W. Bauer, Angular and linear momentum of excited ferromagnets, Phys. Rev. B **88**, 144413 (2013).

[29] E. G. Tveten, A. Qaiumzadeh, and A. Brataas, Antiferromagnetic Domain Wall Motion Induced by Spin Waves, Phys. Rev. Lett. **112**, 147204 (2014).

[30] W. Yu, J. Lan, and J. Xiao, Polarization-selective spin wave driven domain-wall motion in antiferromagnets, Phys. Rev. B **98**, 144422 (2018).

[31] H. Yang, H. Y. Yuan, M. Yan, H. W. Zhang, and P. Yan, Atomic antiferromagnetic domain wall propagation beyond the relativistic limit, Phys. Rev. B **100**, 024407 (2019).

[32] P. Machon, M. Eschrig, and W. Belzig, Nonlocal Thermoelectric Effects and Nonlocal Onsager Relations in a Three-Terminal Proximity-Coupled Superconductor-Ferromagnet Device, Phys. Rev. Lett. **110**, 047002 (2013).

[33] A. Ozaeta, P. Virtanen, F. S. Bergeret, and T. T. Heikkilä, Predicted Very Large Thermoelectric Effect in Ferromagnet-Superconductor Junctions in the Presence of a Spin-Splitting Magnetic Field, Phys. Rev. Lett. **112**, 057001 (2014).

[34] P. Machon, M. Eschrig, and W. Belzig, Giant thermoelectric effects in a proximity-coupled superconductor–ferromagnet device, New J. Phys. **16**, 073002 (2014).

[35] S. Kolenda, M. J. Wolf, and D. Beckmann, Observation of Thermoelectric Currents in High-Field Superconductor-Ferromagnet Tunnel Junctions, Phys. Rev. Lett. **116**, 097001 (2016).

[36] S. Kolenda, C. Sürgers, G. Fischer, and D. Beckmann, Thermoelectric effects in superconductor-ferromagnet tunnel junctions on europium sulfide, Phys. Rev. B **95**, 224505 (2017).

[37] S. Kolenda, P. Machon, D. Beckmann, and W. Belzig, Nonlinear thermoelectric effects in high-field superconductor-ferromagnet tunnel junctions, Beilstein J. Nanotechnol. **7**, 1579 (2016).

[38] P. M. Tedrow, J. E. Tkaczyk, and A. Kumar, Spin-Polarized Electron Tunneling Study of an Artificially Layered Superconductor with Internal Magnetic Field: EuO-Al, Phys. Rev. Lett. **56**, 1746 (1986).

[39] X. Hao, J. S. Moodera, and R. Meservey, Thin-Film Superconductor in an Exchange Field, Phys. Rev. Lett. **67**, 1342 (1991).

[40] F. S. Bergeret, M. Silaev, P. Virtanen, and T. T. Heikkilä, Colloquium: Nonequilibrium effects in superconductors with a spin-splitting field, Rev. Mod. Phys. **90**, 041001 (2018).

[41] T. T. Heikkilä, M. Silaev, P. Virtanen, and F. S. Bergeret, Thermal, electric and spin transport in superconductor/ferromagnetic-insulator structures, Prog. Surf. Sci. **94**, 100540 (2019).

[42] I. V. Bobkova, A. M. Bobkov, and W. Belzig, Thermally induced spin-transfer torques in superconductor/ferromagnet bilayers, Phys. Rev. B **103**, L020503 (2021).

[43] A. Kamra, A. Rezaei, and W. Belzig, Spin Splitting Induced in a Superconductor by an Antiferromagnetic Insulator, Phys. Rev. Lett. **121**, 247702 (2018).

[44] W. Zhang, M. E. Bowden, and K. M. Krishnan, Competing effects of magnetocrystalline anisotropy and exchange bias in epitaxial Fe/IrMn bilayers, Appl. Phys. Lett. **98**, 092503 (2011).

[45] P. Kappenberger, S. Martin, Y. Pellmont, H. J. Hug, J. B. Kortright, O. Hellwig, and E. E. Fullerton, Direct Imaging and Determination of the Uncompensated Spin Density in Exchange-Biased CoO/(CoPt) Multilayers, Phys. Rev. Lett. **91**, 267202 (2003).

[46] L. C. Sampaio, A. Mougin, J. Ferré, P. Georges, A. Brun, H. Bernas, S. Poppe, T. Mewes, J. Fassbender, and B. Hillebrands, Probing interface magnetism in the FeMn/NiFe exchange bias system using magnetic second-harmonic generation, Europhys. Lett. **63**, 819 (2003).

[47] J. Camarero, J. Miguel, J. B. Goedkoop, J. Vogel, F. Romanens, S. Pizzini, F. Garcia, J. Sort, B. Dieny, and N. B. Brookes, Magnetization reversal, asymmetry, and role of uncompensated spins in perpendicular exchange coupled systems, Appl. Phys. Lett. **89**, 232507 (2006).

[48] S. Roy, M. R. Fitzsimmons, S. Park, M. Dorn, O. Petracic, I. V. Roshchin, Z.-P. Li, X. Batlle, R. Morales, A. Misra, X. Zhang, K. Chesnel, J. B. Kortright, S. K. Sinha, and I. K. Schuller, Depth Profile of Uncompensated Spins in an Exchange Bias System, Phys. Rev. Lett. **95**, 047201 (2005).

[49] V. K. Valev, M. Gruyters, A. Kirilyuk, and Th. Rasing, Direct Observation of Exchange Bias Related Uncompensated Spins at the CoO/Cu Interface, Phys. Rev. Lett. **96**, 067206 (2006).

[50] H. Ohldag, A. Scholl, F. Nolting, E. Arenholz, S. Maat, A. T. Young, M. Carey, and J. Stöhr, Correlation between Exchange Bias and Pinned Interfacial Spins, Phys. Rev. Lett. **91**, 017203 (2003).

[51] P. Blomqvist, K. M. Krishnan, S. Srinath, and S. G. E. te Velthuis, Magnetization processes in exchange-biased MnPd/Fe bilayers studied by polarized neutron reflectivity, J. Appl. Phys. **96**, 6523 (2004).

[52] C. Mathieu, M. Bauer, B. Hillebrands, J. Fassbender, G. Güntherodt, R. Jungblut, J. Kohlhepp, and A. Reinders, Brillouin light scattering investigations of exchange biased (110)-oriented NiFe/FeMn bilayers, J. Appl. Phys. **83**, 2863 (1998).

[53] F. Hellman, A. Hoffmann, Y. Tserkovnyak, G. S. D. Beach, E. E. Fullerton, C. Leighton, A. H. MacDonald, D. C. Ralph, D. A. Arena, H. A. Dürr, P. Fischer, J. Grollier, J. P. Heremans, T. Jungwirth, A. V. Kimel, B. Koopmans, I. N. Krivorotov, S. J. May, A. K. Petford-Long, J. M. Rondinelli, N. Samarth, I. K. Schuller, A. N. Slavin, M. D. Stiles, O. Tchernyshyov, A. Thiaville, and B. L. Zink, Interface-induced phenomena in magnetism, Rev. Mod. Phys. **89**, 025006 (2017).

[54] D. S. Rabinovich, I. V. Bobkova, and A. M. Bobkov, Anomalous phase shift in a Josephson junction via an antiferromagnetic interlayer, Phys. Rev. Res. **1**, 033095 (2019).

[55] E. Erlandsen, A. Kamra, A. Brataas, and A. Sudbø, Enhancement of superconductivity mediated by antiferromagnetic squeezed magnons, Phys. Rev. B **100**, 100503 (2019).

[56] Ø. Johansen, A. Kamra, C. Ulloa, A. Brataas, and R. A. Duine, Magnon-Mediated Indirect Exciton Condensation through Antiferromagnetic Insulators, Phys. Rev. Lett. **123**, 167203 (2019).

[57] L. G. Johnsen, S. H. Jacobsen, and J. Linder, Magnetic control of superconducting heterostructures using compensated antiferromagnets, Phys. Rev. B **103**, L060505 (2021).

[58] A. Kamra and W. Belzig, Spin Pumping and Shot Noise in Ferrimagnets: Bridging Ferro- and Antiferromagnets, Phys. Rev. Lett. **119**, 197201 (2017).

[59] A. Kamra, R. E. Troncoso, W. Belzig, and A. Brataas, Gilbert damping phenomenology for two-sublattice magnets, Phys. Rev. B **98**, 184402 (2018).

[60] H. Y. Yuan, Q. Liu, K. Xia, Z. Yuan, and X. R. Wang, Proper dissipative torques in antiferromagnetic dynamics, Europhys. Lett. **126**, 67006 (2019).

[61] K. Chen and S. Zhang, Spin Pumping in the Presence of Spin-Orbit Coupling, Phys. Rev. Lett. **114**, 126602 (2015).

[62] S. A. Bender and Y. Tserkovnyak, Interfacial spin and heat transfer between metals and magnetic insulators, Phys. Rev. B **91**, 140402 (2015).

[63] X.-P. Zhang, F. S. Bergeret, and V. N. Golovach, Theory of spin Hall magnetoresistance from a microscopic perspective, Nano Lett. **19**, 6330 (2019).

[64] M. Eschrig, Distribution functions in nonequilibrium theory of superconductivity and Andreev spectroscopy in unconventional superconductors, Phys. Rev. B **61**, 9061 (2000).

[65] M. Eschrig, Scattering problem in nonequilibrium quasiclassical theory of metals and superconductors: General boundary conditions and applications, Phys. Rev. B **80**, 134511 (2009).

[66] G. S. D. Beach, C. Knutson, C. Nistor, M. Tsoi, and J. L. Erskine, Nonlinear Domain-Wall Velocity Enhancement by Spin-Polarized Electric Current, Phys. Rev. Lett. **97**, 057203 (2006).

[67] J. Mendil, M. Trassin, Q. Bu, J. Schaab, M. Baumgartner, C. Murer, P. T. Dao, J. Vijayakumar, D. Bracher, C. Bouillet, C. A. F. Vaz, M. Fiebig, and P. Gambardella, Magnetic properties and domain structure of ultrathin yttrium iron garnet/Pt bilayers, Phys. Rev. Mater. **3**, 034403 (2019).

[68] O. A. Tretiakov, D. Clarke, G.-W. Chern, Y. B. Bazaliy, and O. Tchernyshyov, Dynamics of Domain Walls in Magnetic Nanostrips, Phys. Rev. Lett. **100**, 127204 (2008).

[69] D. J. Clarke, O. A. Tretiakov, G.-W. Chern, Y. B. Bazaliy, and O. Tchernyshyov, Dynamics of a vortex domain wall in a magnetic nanostrip: Application of the collective-coordinate approach, Phys. Rev. B **78**, 134412 (2008).